Earth and Planetary Science Letters 541 (2020) 116277

Contents lists available at ScienceDirect

Earth and Planetary Science Letters

www.elsevier.com/locate/epsl

The impact of oblique inheritance and changes in relative plate motion on the development of rift-transform systems

G.P. Farangitakis [a,*], P.J. Heron [a], K.J.W. McCaffrey [a], J. van Hunen [a], L.M. Kalnins [b]

[a] Department of Earth Sciences, Durham University, Science Site, Durham, DH1 3LE, UK
[b] School of GeoSciences, University of Edinburgh, The King's Buildings, Edinburgh, EH9 3FE, UK

ARTICLE INFO

Article history:
Received 11 October 2019
Received in revised form 4 April 2020
Accepted 12 April 2020
Available online xxxx
Editor: R. Bendick

Keywords:
structural inheritance
relative plate rotation
transtension
transpression
oblique rifting

ABSTRACT

In transform margins, oblique structural inheritance and plate motion vector changes have a direct impact on the margin's morphology and duration of transform activity. We investigate the effect of these two factors using numerical modelling. To simulate oblique inheritance in continental lithosphere, we model an initial rift-transform-rift configuration oriented at a range of angles (-45^{o} to $+45^{o}$) with respect to the extension direction. In a second suite of calculations, we first extend a rift-transform-rift system orthogonally and then vary the extension direction to simulate rotation of the far-field stress directions, and hence the relative plate motion. We found that transpressional deformation on the transform results in increased duration of fault activity and diffuse, longer transform zones at higher angles, while the opposite is true for the transtensional case. These observations are in good agreement with natural examples such as the Ungava Transform Zone, the Gulf of California and the Gulf of Aden, indicating that relative plate rotation plays an important role in the structural evolution of transform margins. Finally, we present a metric that links current transform margin morphology to past evolution.

1. Introduction

Transform margins and their accompanying transform faults are a relatively understudied feature of plate boundaries that accommodate predominantly boundary-parallel relative plate motion. Initially, they were investigated from a morphological perspective as features that accommodate oceanic spreading (e.g., Wilson, 1965; Le Pichon and Hayes, 1971) and, subsequently, by more complex thermo-mechanical models that investigated their evolution (e.g., Basile, 2015; Mercier de Lépinay et al., 2016). Continent-ocean transforms are found in settings where there has been: a) orthogonal extension between oceanic spreading segments (e.g., Gerya, 2013; Basile, 2015); b) oblique extension (e.g., Bellahsen et al., 2013; Brune and Autin, 2013); c) plate rotations (Morrow et al., 2019); or d) combinations of the above (Farangitakis et al., 2019). Transform margins start their life-cycle as transfer faults offsetting rift segments (Bosworth, 1986) or as proto-transform faults representing diffuse zones of oblique strike-slip motion that initiate during the later stages of continental break-up (Illsley-Kemp et al., 2018). Basile (2015) and Le Pourhiet et al. (2017) refer to these early-stage continental lithosphere faults as "intra-continental transform faults". In this study, we refer to these features as continent-continent transform faults (CCTs), based on the nature of crust being displaced on each side of the margin. Continent-ocean transform faults (COTs) are the structures that link spreading ridges that have evolved from these connecting rifts (Fig. 1a,b). Similarly, continent-ocean fracture zones (COFZs) and some ocean-ocean fracture zones (OOFZs) represent the fossilised remains of transform faults (Fig. 1a). The morphology and duration of activity of a continent-ocean transform margin is linked to tectonic parameters such as the orientation and position of pre-existing lithospheric structures, changes in plate motion vectors, and far-field forces (e.g., Basile, 2015; Le Pourhiet et al., 2017). Around the world, we observe transform faults that can be directly linked with corresponding transform margins (Fig. 1b). However, not all transform faults are directly associated with a transform margin, particularly along segmented spreading ridges (illustrated by the oceanic fracture zone OFZ in Fig. 1b) (Bellahsen et al., 2013; Illsley-Kemp et al., 2018). Our work focuses on the first case: continental transform margins directly associated with transform faults.

Numerous modelling studies indicate that both oblique inheritance and changes in plate motion affect transform margin evolution. Bellahsen et al. (2013) suggest that pre-existing Mesozoic basins and transfer zones partially control the current Gulf of Aden oblique spreading. Basile (2015) shows that continent-ocean trans-

* Corresponding author.
E-mail address: georgios-pavlos.farangitakis@durham.ac.uk (G.P. Farangitakis).

https://doi.org/10.1016/j.epsl.2020.116277

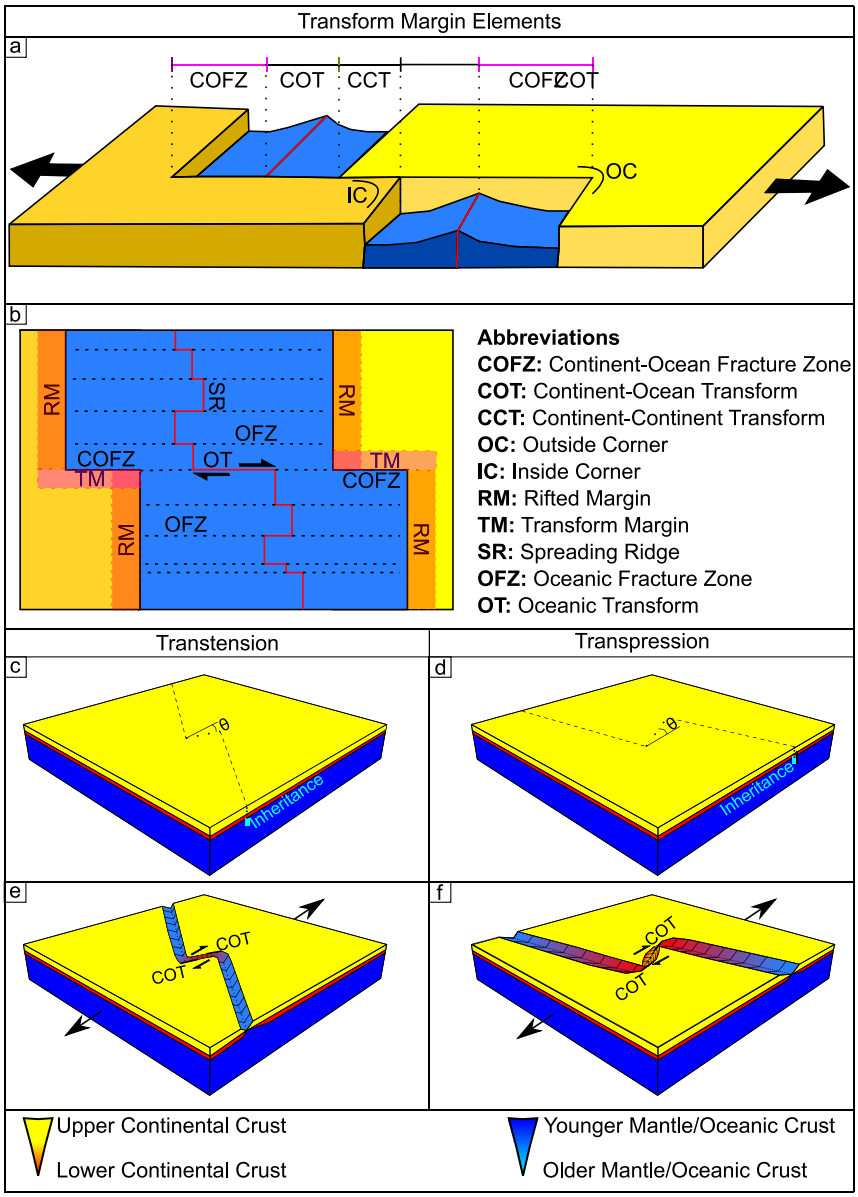

Fig. 1. a: Main elements of an active transform margin profile (redrawn from Lorenzo, 1997). b: Main elements of a passive transform margin (map view). c-f: Schematic representation of the response of an inherited structure to an oblique extensional deformation. c, d: two initial conditions; e, f: transtensional and transpressional deformation on transform segment after extension/rifting. Cyan feature in the mantle in c and d represents the inherited feature projected onto the surface with a dashed black line. θ: angle of rotation between the extension direction and the transform segment. (For interpretation of the colours in the figure(s), the reader is referred to the web version of this article.)

form faults develop within continental lithosphere either by reactivating or cross-cutting pre-existing structural features. Farangitakis et al. (2019) demonstrate how changes in relative plate motion produce oblique rifts accompanied by transtension (Gulf of California) or transpression (Tanzania Coastal Basin) along transform margins. Ammann et al. (2018) argue that formation of long transform faults (such as those in the Central Atlantic) is favoured by high obliquity and slow extension rates during continental rifting. Peace et al. (2017) indicate lithosphere inheritance could strongly control the evolution of an obliquely rifted margin in W. Greenland, while numerical modelling of the region inferred ancient mantle scarring may also play a role (Heron et al., 2019).

By analysing a global rift database, Brune et al. (2018) suggested that oblique rifting might actually be the rule, rather than the exception. If so, the corresponding transform margins must also experience significant transtensional or transpressional deformation (Figs. 1c-f), which would influence their morphology and be evident in many natural examples across the world.

In this study, we explore the overall effect of inherited obliquity and change in relative plate motion on continent-ocean transform margins through a series of numerical modelling experiments. The first set investigates how the obliquity of a pre-existing zone of weakness within the continental lithosphere affects continent-ocean transform margin evolution. The second set examines the role that a change in relative plate motion plays in margin evolution. We then link our observations to continent-ocean transform margins around the world. Our modelling focuses on the continental crust and therefore does not take into consideration oceanic crustal features; hence, our observations are focused on the evolution of the continental parts of the transform margins and stop when these become passive. Finally, we present a novel approach for linking transform margins' current morphology to their past evolution.

Table 1
Physical properties of the models (parameters obtained from a: Rutter and Brodie, 2004; b: Rybacki et al., 2006; c: Hirth and Kohlstedt, 2004; d: Heron et al., 2019; e: Naliboff and Buiter, 2015; f: Chapman, 1986).

Parameter	Unit	Upper Crust	Lower Crust	Mantle	Seed
Rheology		Wet Quartzite[a]	Wet Anorthite[b]	Dry Olivine[c]	Dry Olivine[c]
Thermal diffusivity[d]	m^2/s	1.19×10^{-6}	1.15×10^{6}	1.33×10^{-6}	1.33×10^{-6}
Density[e]	kg/m^3	2.8×10^{3}	2.9×10^{3}	3.3×10^{3}	3.3×10^{3}
Thermal expansivity[d]	1/K	2.00×10^{-5}	2.00×10^{-5}	2.00×10^{-5}	2.00×10^{-5}
Internal friction angles[d]	degrees	20	20	20	0
Cohesions[d]	Pa	2.00×10^{7}	2.00×10^{7}	2.00×10^{7}	1.00×10^{7}
Plasticity strain weakening interval[d]		0-0.5	0-0.5	0-0.5	0-0.5
Temperature at top of layer[f]	K	273 (top)	681.6 (top)	823 (top)	
Heat production[f]	W/m^3	1.50×10^{-6}	0	0	0
Thermal conductivity[f]	W/(m*K)	2.5	2.5	3.3	3.3
Viscosity range[e]	Pa s	1.00×10^{18}–1.00×10^{26}	1.00×10^{18}–1.00×10^{26}	1.00×10^{18}–1.00×10^{26}	1.00×10^{18}–1.00×10^{26}

2. Methodology

The 3D nature of continent-ocean transform margins and the interplay between local and far-field kinematic, dynamic and transient effects pose a challenge for both numerical and analogue models. Thus far, modelling of transform margins and the parameters that affect their evolution has followed two approaches. The first examines the development of rift connectivity by placing isolated seeds in the lithosphere (either as zones of weakness or as modified Lithosphere-Asthenosphere Boundaries/LABs) and studying their interactions by varying their location (e.g., overlap, underlap), shape and orientation within an extensional model (e.g., Allken et al., 2012; Gerya, 2013; Zwaan and Schreurs, 2017; Le Pourhiet et al., 2017; Illsley-Kemp et al., 2018). The second modelling approach examines the deformation of already established shear zones or connected rift segments and how they respond to changes in extension direction or oblique rifting (e.g., Brune et al., 2012; Brune and Autin, 2013) or to inherited structures situated at oblique angles to the established rifts (Autin et al., 2013).

Following the second approach, we use two different experimental scenarios to investigate the effects of obliquity of inherited structures and plate rotations on a rift-transform-rift configuration in 3D space. Computations were carried out using the open source finite element numerical code ASPECT, version 2.1.0 (Kronbichler et al., 2012; Heister et al., 2017) and follow the study of Heron et al. (2019). Our models are governed by a dislocation creep flow law and display Drucker-Prager plasticity as a rheology with strain weakening (e.g., Naliboff and Buiter, 2015, Table 1), using a "seed" configuration that represents an initial weak zone in the top of the mantle (Huismans and Beaumont, 2011).

2.1. Experimental setup

We use a box with dimensions of 800 by 800 km horizontally and 120 km vertically. Compositionally, the top 20 km is initially upper continental crust, with 10 km lower continental crust beneath and 90 km of mantle lithosphere at the bottom (Fig. 2).

Resolution is uniform with 3.125 × 3.125 × 3.125 km per cell, totalling 262,144 active cells and 19 million degrees of freedom. Our models have prescribed boundary velocity conditions on their $x = 0$ km, $x = 800$ km and $z = 120$ km boundaries and tangential velocity boundary conditions on the $y = 0$ km and $y = 800$ km boundaries. The top boundary has a free surface, which allows for topography and is generated by an Arbitrary Lagrangian-Eulerian framework with 848691 degrees of freedom (Rose et al., 2017). The applied east-west extension is 1 cm/yr on each boundary (total of 2 cm/yr), and outflow on these edges is balanced by an inflow of 0.3 cm/yr at the base.

2.2. Seed configuration and obliquity

We introduce a simple left-stepping rift-transform-rift configuration, represented by a weak seed 2 km beneath the base of the crust straddling the horizontal midpoint (Fig. 2). The seed is used as an inherited structure in the first set of experiments. In the second set, the seed is used to initiate orthogonal rifting that replicates the control experiment (Fig. 2b) and is then rotated after 5 Myr. The rift seeds extend the full length of the box (even when rotated). We use a rift segment offset of 160 km, intermediate between the values used by Allken et al. (2012) and Le Pourhiet et al. (2017). We tested offsets between 120-200 km (Suppl Figures S1-S5) and find that transform faults are established at these offset lengths as well. We define positive angle change as clockwise obliquity between seed and extension direction, creating transtension (as in Fig. 2c) on the transform fault, and negative angle change as counter-clockwise obliquity, creating transpression (as in Fig. 2d). The models are then computed in the two different scenarios: one featuring inherited structures oblique to the extension direction and another that simulates rotation in relative plate motion.

2.2.1. Inheritance experiments

The models start from $t_0 = 0$ Myr with an inherited seed (e.g., Fig. 2c). First, we conduct a control experiment with the rift-transform-rift configuration orthogonal (0^o) to the extension direction (Figs. 2b and 3). We then perform 10 further experiments, with the seed at 10^o obliquity intervals from $\theta = -5^o$ to -45^o and 5^o to 45^o, representing increasingly oblique inherited structures (Fig. 2c).

2.2.2. Effect of rotation experiments

In a second set of experiments, we use a three-step process to evaluate the effect of an imposed rotation of plate motion vectors on an existing continent-ocean transform. First, we calculate a 1200×1200×120 km orthogonal model with the same seed set-up as the control model shown in Fig. 2b. The 5 Myr output of the larger 3D model is used as a "sampling box" of the temperature, composition (upper crust, lower crust, and mantle), seed and total strain rate after 5 Myr. We then rotate the box by the desired angle and sample a smaller 800×800×120 km domain around its 3D midpoint. The established spreading system now sits at an angle to the extension direction in this smaller domain. The rotation values range from $\theta = -45^o$ to -5^o and 5^o to 45^o, respectively (see Suppl. Material code repository). Finally, we use this new smaller domain as an initial composition and temperature field to run a suite of experiments on delayed rotation (Fig. 2d).

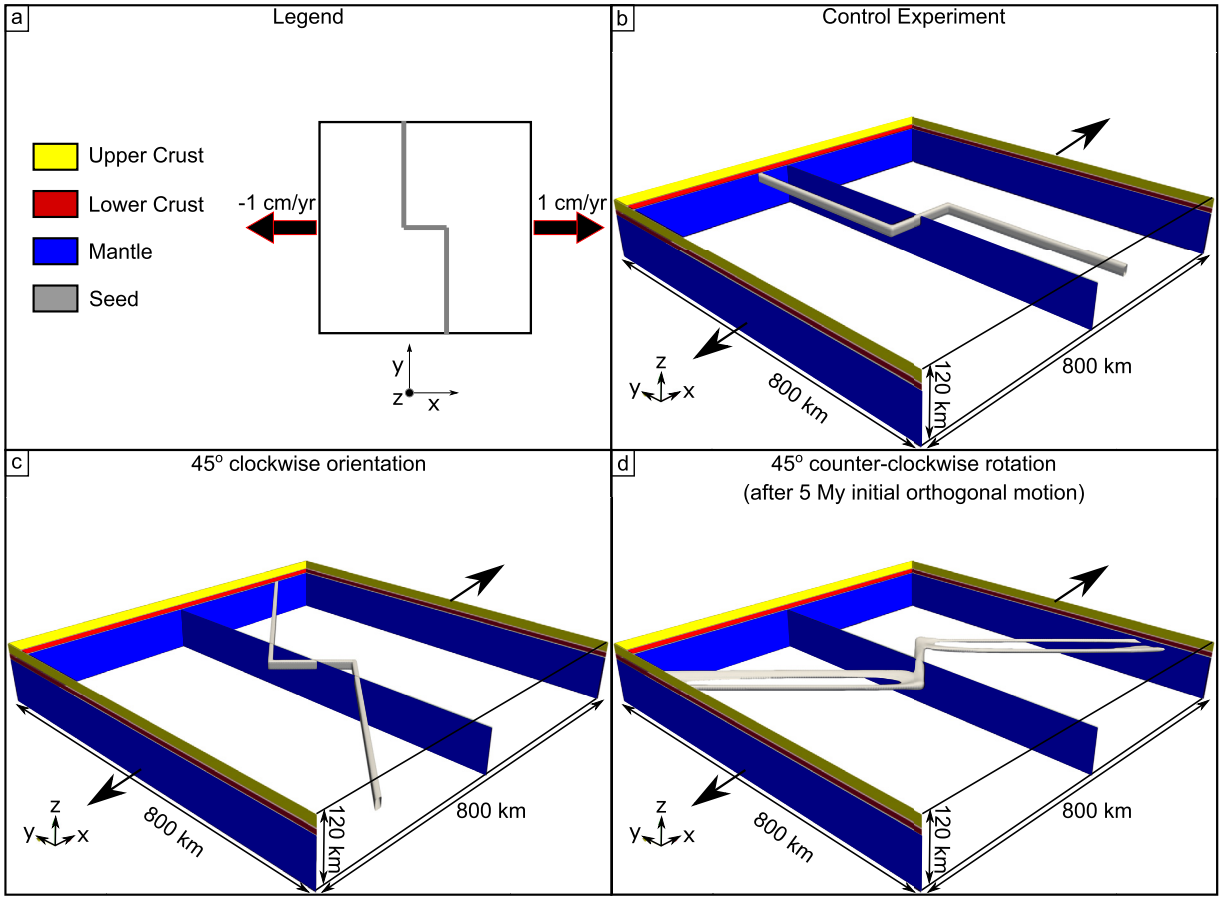

Fig. 2. Experimental set up. a: rheology and model set-up, b: control experiment configuration, c: obliquity experiment example set-up for transtension on transform boundary, d: set-up to simulate rotation of plate vectors, which creates transpression on the transform boundary following an initial orthogonal extension.

2.3. Governing equations

This study is governed by the equations of conservation of momentum, mass and energy in an incompressible medium with an infinite Prandtl number:

$$-\nabla \cdot (2\mu\dot{\varepsilon}) + \nabla P = \rho g \tag{2.1}$$

where μ = viscosity, $\dot{\varepsilon}$ = strain rate tensor, P = pressure, ρ = density and g = gravitational acceleration.

$$\nabla \cdot u = 0 \tag{2.2}$$

$$\rho C_p \left(\frac{\partial T}{\partial t} + u \cdot \nabla T \right) - \nabla \cdot k \nabla T = \rho H \tag{2.3}$$

where u = velocity vector, C_p = thermal heat capacity, T = temperature, t = time, k = thermal conductivity, and H = internal heat production.

Upper crust, lower crust, mantle and seed represent compositional fields that adhere to the pure advection equation:

$$\frac{\partial C_i}{\partial t} + u \cdot \nabla C_i = 0 \tag{2.4}$$

where C_i = compositional field.

The above equations are solved with the finite element method in a discretised domain of finite elements using an iterative Stokes solver (Kronbichler et al., 2012). The solution is then interpolated using Lagrangian polynomials as basis functions (Glerum et al., 2018). The models use a temperature-dependent density, but no pressure-dependence, since the model is incompressible (e.g., Heron et al., 2019).

The models have a nonlinear viscous flow (dislocation creep) with Drucker-Prager plasticity for the rheology, a setup used in many previous studies (e.g., Huismans and Beaumont, 2011; Naliboff and Buiter, 2015; Heron et al., 2019).

Dislocation creep is defined as:

$$\mu = 0.5 A^{-\frac{1}{n}} \dot{\varepsilon}_e^{\frac{(1-n)}{n}} \exp\left(\frac{E + PV}{nRT}\right) \tag{2.5}$$

where A = viscosity prefactor, n = stress exponent ($n > 1$), $\dot{\varepsilon}_\mathrm{e}$ = square root of the deviatoric strain rate tensor second invariant, E = activation energy, V = activation volume and R = universal gas constant (Karato, 2008).

Viscosity is limited through a Drucker-Prager yield criterion where the yield stress in 3D is:

$$\sigma_y = (6C\cos\varphi + 2P\sin\varphi) / \left(\sqrt{3}\,(3 + \sin\varphi)\right) \tag{2.6}$$

where C = cohesion and φ = angle of internal friction. When φ equals 0, as in the imposed seed, the yield stress is fixed and equal to the Von Mises yield criterion. When the viscous stress ($2\mu\dot{\varepsilon}_\mathrm{e}$) exceeds the yield stress σ_y, we apply plastic yielding by rescaling the effective viscosity (Willett, 1992; Kachanov, 2004) so that the stress is less than the yield value (e.g., Thieulot, 2011). To ensure numerical stability, we constrain the viscosity in our models between 10^{18} and 10^{26} Pa·s (Table 1).

We apply strain weakening for the internal friction angle and cohesion. They reduce linearly as a function of finite strain magnitude to 50% of their initial value at a strain of 50% (Table 1; Bos and Spiers, 2002; Heron et al., 2019). Our sensitivity analysis for strain weakening parameters (Suppl. Figures S6-S11) indicates

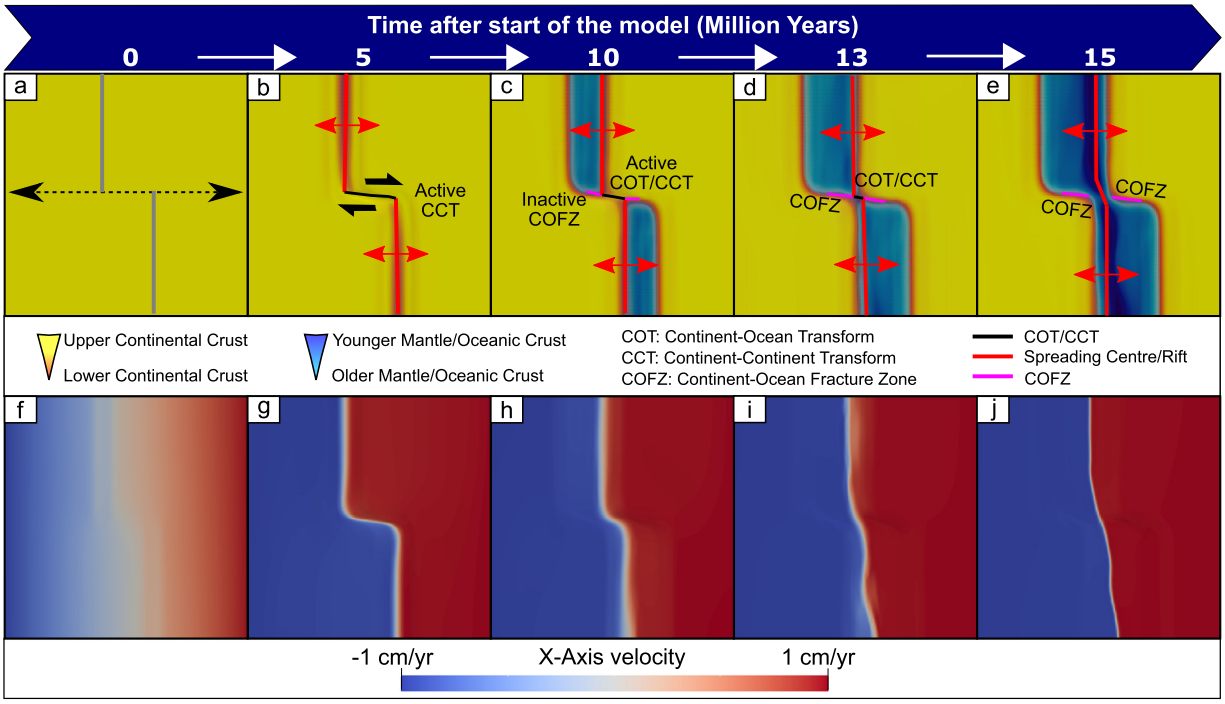

Fig. 3. Orthogonal extension control model. a-e: Individual panels show surface material evolution through time. Location of seeds (grey lines) and extension direction (dashed arrows) shown in panel a. f-j: surface velocity in the *x* direction. For an uninterpreted version, strain rate patterns and cross-sections across the rifted margins, refer to Suppl. Figures S14-S16.

that no significant changes in the margin morphology occur, apart from when the internal angle of friction of the seed is increased (Suppl. Figures S7 & S9). This change is expected since the rheological weakness that the seed represents is diminished, so the models resemble the result of the pure orthogonal rifting case.

The model compositional fields have individual values of thermal and rheological parameters (Table 1). If more than one compositional fields are present at the same time within a cell, viscosities are averaged harmonically (Glerum et al., 2018). We use a rheological setup similar to that of Naliboff and Buiter (2015), using wet quartzite flow laws for the upper crust (Rutter and Brodie, 2004), wet anorthite for the lower crust (Rybacki et al., 2006), and dry olivine for the mantle (Hirth and Kohlstedt, 2004). The modelling set-up does not allow for the formation of brittle oceanic crust, but instead keeps the rheology of the mantle. Thus, we focus our observations on the continental crust aspects of the models.

2.4. Thermal model set-up

We prescribe an initial temperature field similar to a typical continental geotherm (Chapman, 1986) with no lateral variations:

$$T(z) = T_o + \frac{q}{k}z - \frac{Hz^2}{2k} \tag{2.7}$$

where T_0 = surface temperature of each layer, H = heat production, q = heat flow through the surface of the specific layer, k = thermal conductivity and z = depth (see Table 1). Our sensitivity analysis for layer temperature parameters indicates no effect on the transform margin evolution timing. However, a colder top mantle surface increases the effect of the seed on the rifted margin asymmetry (see Suppl. Figures S12-S13).

3. Results

Our experimental results on the early development of transform margins are presented as maps of the surface evolution of the model. We also consider the kinematics observed in the surface velocity plots and evolving surface material. We first present the control orthogonal experiment (Fig. 3). We then present two sets of models (each with 5 experiments) for transtension (positive θ angles) (Figs. 4 & 5), followed by two more sets for transpression (negative θ angles) (Figs. 6 & 7). The first set in each case (Figs. 4 & 6) represents oblique inheritance, while the second (Figs. 5 & 7) represents a change in the relative plate motion vector after 5 Myr of orthogonal extension. In each figure, the seed configuration and direction of extension are shown in the first panel. Surface strain rate and surface velocity plots are presented in Suppl. Figures S15-32 and further analysed in the discussion.

3.1. Development of structures (orthogonal extension)

In our control experiment, rifting initiates from the outer edges of the box, perpendicular to the extension direction (Fig. 3b), and propagates towards the transform seed. Transform motion is expressed first as a continent-continent transform fault (CCT) followed by a continent-ocean transform fault (COT) (Fig. 3c). In this case, the transform margin is active until 13 Myr (Fig. 3d); by 15 Myr, the transform margin is expressed by two continent-ocean fracture zones (COFZs) separated by a spreading axis (Fig. 3e).

3.2. Transtensional deformation on the transform boundary (positive angle θ to extension direction)

3.2.1. Oblique inheritance experiments

Fig. 4 shows the extension of a rift-transform-rift configuration oriented at a positive obliquity angle (with respect to the extension direction) between 5-45°. The transform structure undergoes transtensional deformation, which is illustrated by snapshots every 5 Myr from the initiation of extension. The duration of activity on the COTs and CCTs depends on the obliquity of the inherited structure, decreasing with increasing θ. For 5°, the transform margin is active until 12.5 Myr from the start of the model (Fig. 4c);

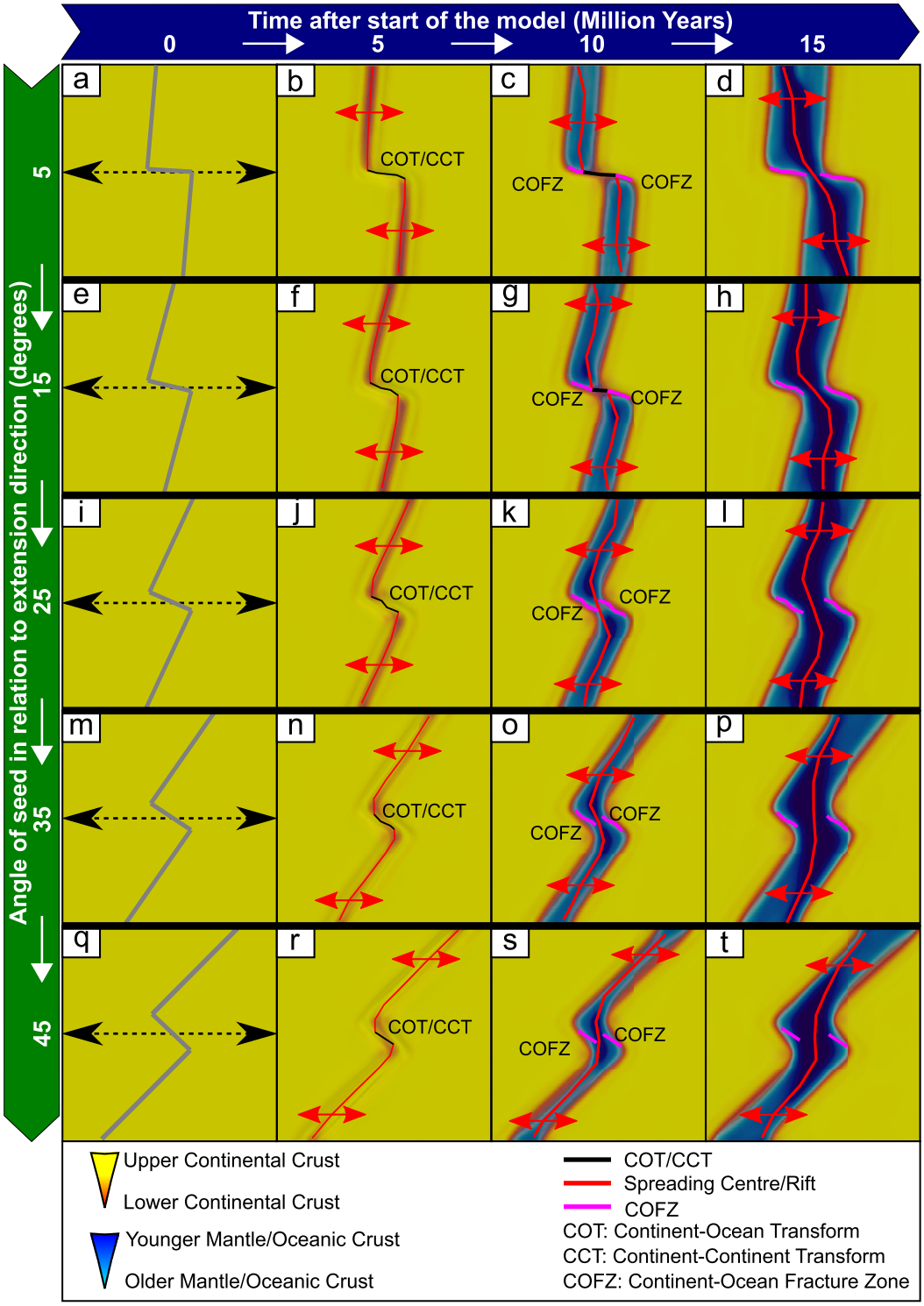

Fig. 4. Transtensional oblique inheritance models, with a seed oriented at a positive θ (with respect to the extension direction). Individual panels show surface material evolution through time. Location of seeds (grey lines) and extension direction (dashed arrows) shown in panels a,e,i,m,q. For an uninterpreted version, strain rate patterns, velocity plots and cross-sections across the rifted margins, refer to Suppl. Figures S17-S20.

for 15°, until 11 Myr (Fig. 4g); for 25°, until 9 Myr (Fig. 4j); for 35°, until 7.5 Myr (Fig. 4n); and for 45°, until 7 Myr (Fig. 4r). After these times, the COTs become inactive COFZs (pink lines in Fig. 4). In comparison to the 5°, 15° and 25° experiments (Fig. 4a,e,i), the 35° and 45° experiments also produce a shorter transform segment connecting the two rifts (Fig. 4n,r). Spreading localisation also depends on the angle of the inherited structure. At 5°, spreading localises in a quasi-uniform manner above the inherited rift structures. As obliquity increases, spreading increasingly localises near the transform seed first before spreading along the rift segments (darker mantle colourations on either side of the spreading ridges in Fig. 4 at 10 Myr) (Suppl. Figure S17).

3.2.2. Rotation experiments

We next present our experiments simulating a change in relative plate motion after rifting initiation (Fig. 5). We perform or-

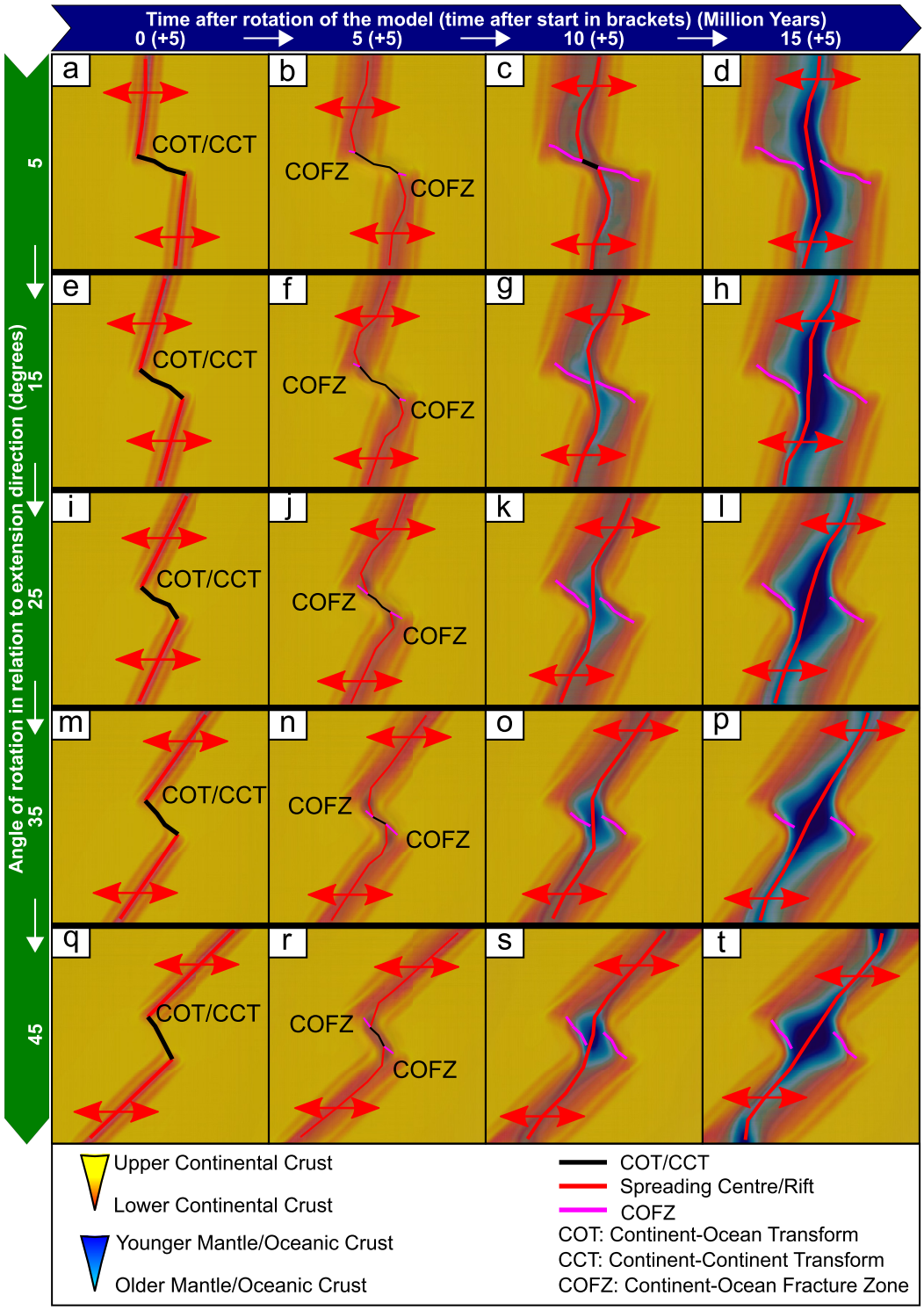

Fig. 5. Transtensional rotated models with a positive θ of rotation (with respect to the extension direction) after an initial 5 Myr of orthogonal extension. Individual panels show surface material evolution through time. For an uninterpreted version, strain rate patterns, velocity plots and cross-sections across the rifted margins, refer to Suppl. Figures S21-S24.

thogonal rifting for 5 Myr and then change the extension direction by 10° increments from 5° to 45°. As marked in Fig. 5, all model snapshots refer to the start of rotation after the initial rifting (e.g., Fig. 5a is 0 Myr + 5 Myr of initial rotation). In all models, spreading initiates at the outside corners of the rift-transform configuration, with a sigmoidal shape at the smaller angles (Fig. 5c,g,k). As the angle increases, this sigmoidal shape progressively becomes rhomboidal (Figs. 5o,s) (see also darker mantle colorations across both sides of the spreading ridge in Fig. 5 after 15+5 Myr and Suppl. Figure S19).

COT and CCT activity time again are influenced by the angle of rotation. For 5°, the transform margins are active until 11 Myr after the start of rotation (Fig. 5c); for 15°, until 9.5 Myr (Figs. 5f,g); for 25°, until 8.5 Myr (Figs. 5j,k); for 35°, until 7 Myr (Figs. 5n,o); and for 45°, until 6 Myr (Figs. 5r,s). After these times, the passive transform margin is represented by COFZs (pink lines in Fig. 5).

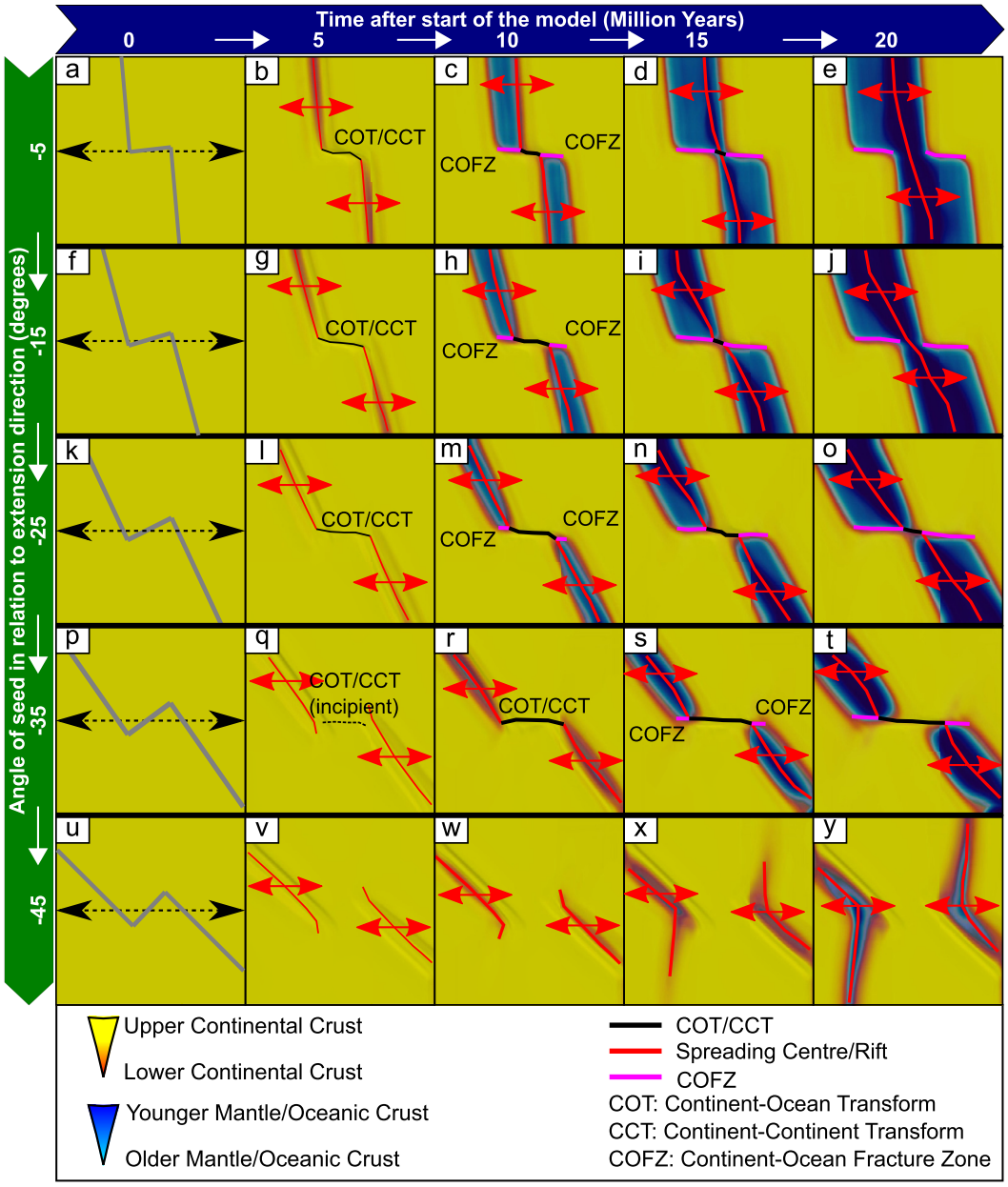

Fig. 6. Transpressional oblique inheritance models, with a seed oriented at a negative θ (with respect to the extension direction). Individual panels show surface material evolution through time. Location of seeds (grey lines) and extension direction (dashed arrows) shown in panels a,f,k,p,u. For an uninterpreted version, strain rate patterns, velocity plots and cross-sections across the rifted margins, refer to Suppl. Figures S25-28.

3.3. Transpressional deformation on the transform boundary (negative angle θ to extension direction)

3.3.1. Oblique inheritance experiments

In the transpressional oblique inheritance experiments, we investigate the case of oblique extension on a rift-transform-rift configuration oriented at a negative angle between -5^o and -45^o (Fig. 6). In all cases, rifting and subsequent spreading localise first at the outer boundaries of the box, perpendicular to the extension direction, and propagate towards the rift-transform corners. CCTs evolve into COTs, accommodating any horizontal motion, except for the -45^o experiment (Fig. 6u-y).

The length of time that the transform boundary remains active again depends on the obliquity of the inherited structure. For -5^o, transform activity lasts until 15 Myr after the start of the model (Fig. 6d); for -15^o, until 17 Myr (Fig. 6i); for -25^o, until 22 Myr (Fig. 6o); and for -35^o, until 40 Myr (Fig. 6t) before becoming inactive COFZs. The -45^o experiment does not form a transform. Instead, the initial rifts propagate towards the centre and then away from each other (Figs. 6v-w) as they evolve into two distinct spreading segments that do not interact (Fig. 6y). The evolution of the -35^o experiment displays a mixture of the tectonic characteristics shown in the -45^o and -25^o experiments. Rifting propagates inwards from the outer boundaries of the box. Although it initially seems that the rift segments are moving away from the transform zone, similar to the -45^o experiment (Fig. 6q), the spreading segments then connect through incipient transform motion (similar to -25^o Fig. 6l) and form an elongate transform zone (Figs. 6r-t and strain rate patterns at 20 Myr in Suppl. Figure S26).

3.3.2. Rotation experiments

We next present the rotated experiments (for transpressional negative angles θ at 10^o increments from -5^o to -45^o) simulat-

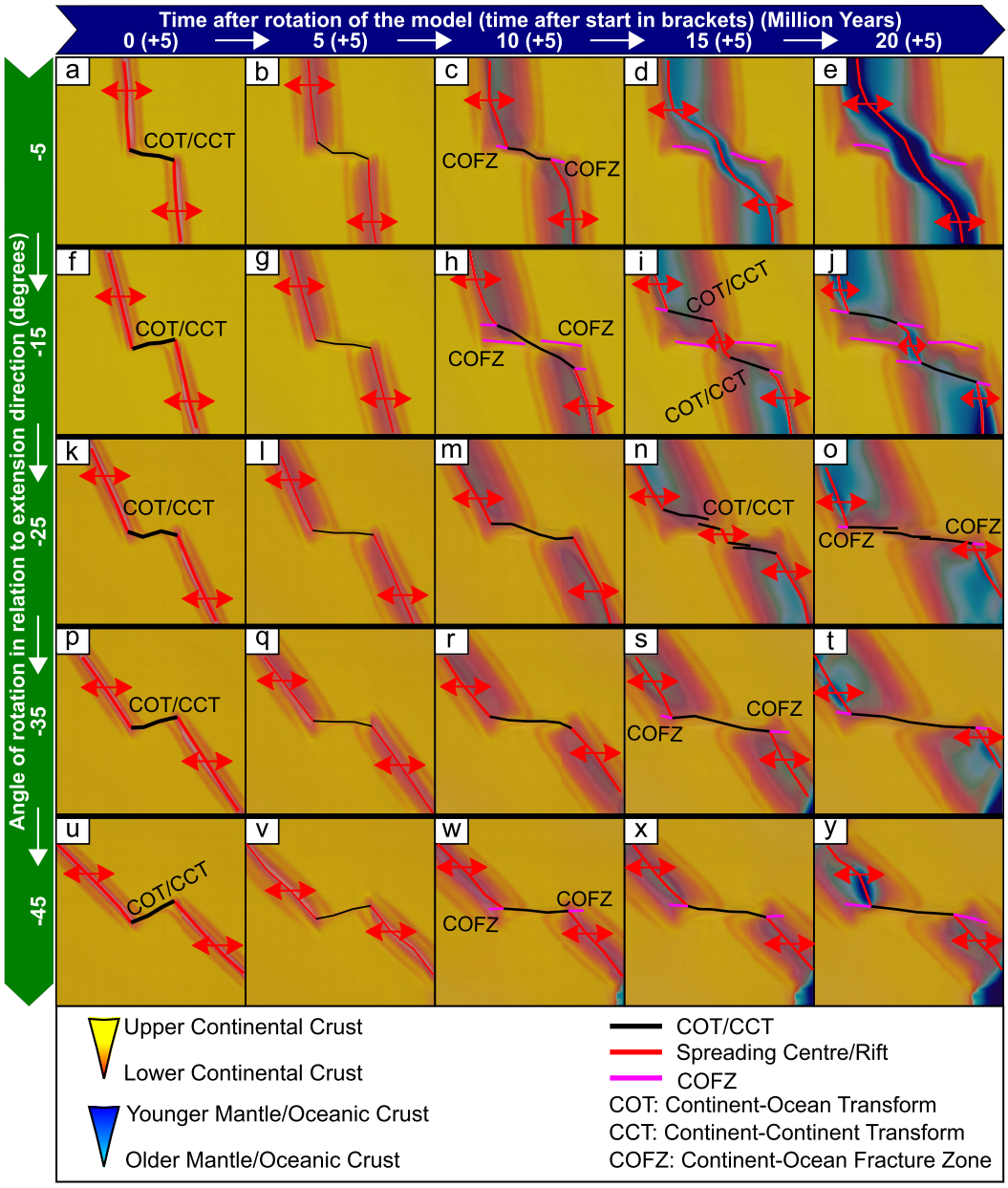

Fig. 7. Transpressional rotated models with a negative θ of rotation (with respect to the extension direction) after an initial 5 Myr of orthogonal extension. Individual panels show surface material evolution through time. For an uninterpreted version, strain rate patterns, velocity plots and cross-sections across the rifted margins, refer to Suppl. Figures S29-S32.

ing a change in relative plate motion after 5 Myr of orthogonal rifting (Fig. 7). Similar to the oblique inheritance case, rifting and spreading localise from the outer boundaries of the box towards the rift-transform corners (note surface material on each side of the rift/spreading ridges in Fig. 7 after 10+5 Myr). The established transform zones accommodate any horizontal motion through CCTs and COTs. Transform activity duration increases with the angle of imposed rotation. For -5^{o}, transform motion is active until 15 Myr after rotation (Fig. 7c); for -15^{o}, until 29 Myr (Fig. 7j); for -25^{o} until 35 Myr (Fig. 7o); and for -35^{o} and -45^{o}, for at least 40 Myr, exceeding the model runtime (Figs. 7t,y). An en-echelon pattern is observed at the surface around the transform zones for the lower rotation angle models (Figs. 7c,d for -5^{o}, 7i-j for -15^{o}, and 7n,o for the -25^{o} experiment). This pattern corresponds to diffuse zones where horizontal motion is accommodated. Within this zone, the transform boundary can be segmented into smaller, shorter lived transforms, such as in the -25^{o} experiment (Fig. 7o) or -15^{o} experiment (Fig. 7j). For a zoomed-in version of the -15^{o} and -25^{o} transpressional rotation experiments accompanied by velocity plots, see Suppl. Figures S33-S34.

By the end of the -5^{o} experiment, spreading follows the rotation angle (Fig. 7e). However, in the -15^{o} model, spreading is focused on 3 segments, connected by oblique diffuse zones (Fig. 7j). Finally, in higher angle models (-25 to -45^{o}), spreading is focused on the inside corners of the rift-transform intersections while the transform faults are still active (Figs. 7o,t,y).

4. Discussion

Our two sets of numerical modelling experiments simulate the effect of a) oblique inheritance and b) a relative plate motion vector change in a rift-transform-rift setting. For both sets, we find that for a left-stepping geometry, a positive angle of rotation

(clockwise) from the extension direction results in transtension, accompanied by oblique rifting and spreading over the corners of the rift-transform-rift configuration (Fig. 4 and 5). For negative (counter-clockwise) angles, where the transform experiences transpressional strain, increased obliquity increases the duration and length of the active transform segment in both the inheritance and relative plate rotation experiments (Fig. 6 and 7). In the following sections we compare our results with natural examples.

4.1. Comparison with natural examples

4.1.1. Ungava Transform Zone, Davis Strait

We correlate our experiments with natural examples around the world (Fig. 8), beginning with the Ungava Transform Zone in the Davis Strait between Canada and W. Greenland. The Ungava Transform Zone is a large right-stepping transform zone that accommodated horizontal motion between (now extinct) oblique spreading ridges in Baffin Bay in the north and the Labrador Sea in the south (Oakey and Chalmers, 2012). Estimates for the obliquity of the rifts relative to spreading direction are poorly constrained, and range from 8-19° for the Labrador Sea, and 25-40° for Baffin Bay between 124-79 Ma (Jeanniot and Buiter, 2018). The area also underwent a 30° clockwise change in its spreading direction around 35 Ma (Doré et al., 2016), resulting in widespread transpression and transtension.

The Ungava Transform Zone has thus experienced both oblique inheritance and later changes in plate motion, but the effects of the most recent phase of deformation, the relative rotation, are likely to be easiest to observe. Therefore, we compare the area with our 25° transpressional rotation model (Figs. 7k-o) (shown mirror-imaged for easier comparison, Fig. 8a). Both our model and the Ungava Transform Zone evolve in a similar way. Opening of the first rifted basins occurs in an orthogonal extension zone, with a continental transform connecting the spreading centres (Oakey and Chalmers, 2012). Once the spreading direction changes and oblique rifting is initiated, the juxtaposed continental crust is forced into transpression (velocity vector arrows in Suppl. Figures S33-34). This results in a zone of transpression onshore W. Greenland (Wilson et al., 2006; Peace et al., 2017) and inversion structures offshore, analogous to the deformation we observe in our numerical model (grey circles marked TP in Fig. 8b). Similarly, in our model, we observe a zone of high compressional stress on the inside corners of the rift-transform intersection (Suppl. Figure S35).

As spreading develops, a wide, transtensional region forms between the north and south Davis Straight spreading segments, the Ungava Transform Zone (Fig. 8b, Reid and Jackson, 1997). Evidence of transtension includes oceanic material found along the transform (Wilson et al., 2006; Oakey and Chalmers, 2012; Peace et al., 2017). In our experiment, we also observed the formation of a diffuse transtensional zone (pink outline in Fig. 8a, see also velocity vector arrows in Suppl. Figures S33-34). Because of the large range of estimates for obliquity and rotation in the Ungava Transform Zone, we also compare it with our 15° rotated model. This model includes a large segmented transform zone (Fig. 7i,j), where transpression takes place in the corners of the rift-transform intersections and transtension occurs within the thinned crust, similar to the Ungava Transform Zone (Fig. 7j).

4.1.2. Gulf of California

A natural example of transtension is the Gulf of California partitioned oblique margin, which undergone a 5-15° rotational change in relative plate motion (Bennett and Oskin, 2014). It formed a series of en-echelon pull-apart basins, which later developed into spreading centres (Umhoefer et al., 2018; Farangitakis et al., 2019) (Fig. 8d). We match this to our 5° transtensional rotated model (Fig. 5a-d), although the Gulf of California also displays similar features to the 15° experiment (Fig. 5e-h). In our experiments, we model a single left-stepping rift-transform-rift system, so we do not replicate the complete architecture of the Gulf of California, but rather how each transtensional pull-apart would evolve. In both cases, the initial evolution begins with a transtensional zone forming near the outside corners of the rift-transform intersections (pink areas in Figs. 8c and 8d). Spreading in our models localises from the rift-transform intersections outwards, which is similar to the evolution of the N. Gulf of California, where spreading is more localised closer to the intersection of the Ballenas Transform Fault Zone and the Lower Delfin Basin spreading centre (Persaud et al., 2003).

4.1.3. Gulf of Aden

Finally, we correlate the rifted margin asymmetry in one of our rotation models with the evolution of the Gulf of Aden, where the transition from continent to ocean is wider in the outside corners of the Alula-Fartak and Socotra-Hadbeen Fracture Zones than in the inside ones (Fig. 8g, orange zones marked COBZ; Bellahsen et al., 2013). Kinematically, the Gulf of Aden has undergone ~35 Myr of spreading (Bellahsen et al., 2013) and is characterised by 3 components: a) oblique crustal inheritance in the form of Mesozoic basins trending ~80-90° clockwise to spreading (Autin et al., 2013); b) an oblique rift and spreading trend oriented 40° clockwise to the direction of plate motion, segmented by left-stepping transform faults; and c) a ~26° change in the plate motion vector reducing rifting obliquity from the previous oblique rifting trend of ~68° observed 20 Myr ago (Bellahsen et al., 2013; Brune and Autin, 2013; Jeanniot and Buiter, 2018). The Gulf of Aden has also been influenced by the Afar hotspot (Leroy et al., 2012), and associated magmatism. However, our models do not take magmatic emplacement into account. Instead, we focus on understanding what features can be explained by just the kinematics and inheritance of the region.

We compare the transition across the spreading centre in the 5° oblique inheritance model (Fig. 8e and inset figure) to the continent-ocean boundary zone along two main fracture zones in the Gulf of Aden (Fig. 8g, orange zones marked COBZ). This model fits two characteristics of the natural example: a) the obliquity of the inherited structures through the general orientation of the seed (green in Fig. 8e) is in accordance with the Mesozoic fabric in the Gulf (green in Fig. 8g); and b) the angular agreement of the spreading trend with respect to the relative plate motion (red lines in Figs. 8e,f,g). The width of transition from continent to oceanic crust is 115 km in the inside and 110 km (~5% shorter) in the outside corners of the rift-transform intersection, which does not agree with the Gulf's margin width.

However, if the 26° transtensional plate motion vector change (Jeanniot and Buiter, 2018) is considered, then the Gulf of Aden can be compared to the 25° positive rotation angle experiment (Fig. 8f and inset figure). Here, the transition from oceanic to undisturbed continental crust is ~120 km in the inside and 260 km (116% longer) in the outside corners of the rift-transform intersection (inset in Fig. 8f). Thus, considering the kinematics of the area (Bellahsen et al., 2013), we can infer that the change in plate motion in the Gulf of Aden is a key contributing factor in the resulting margin asymmetry.

4.2. Rift seed geometry and connectivity

We find that the rift seed spacing used in our study generates a transform margin independent of whether we include a transform seed or not. Our spacing of ~5H (where H is the thickness of the continental crust) produces transform linkage (Fig. 3 and

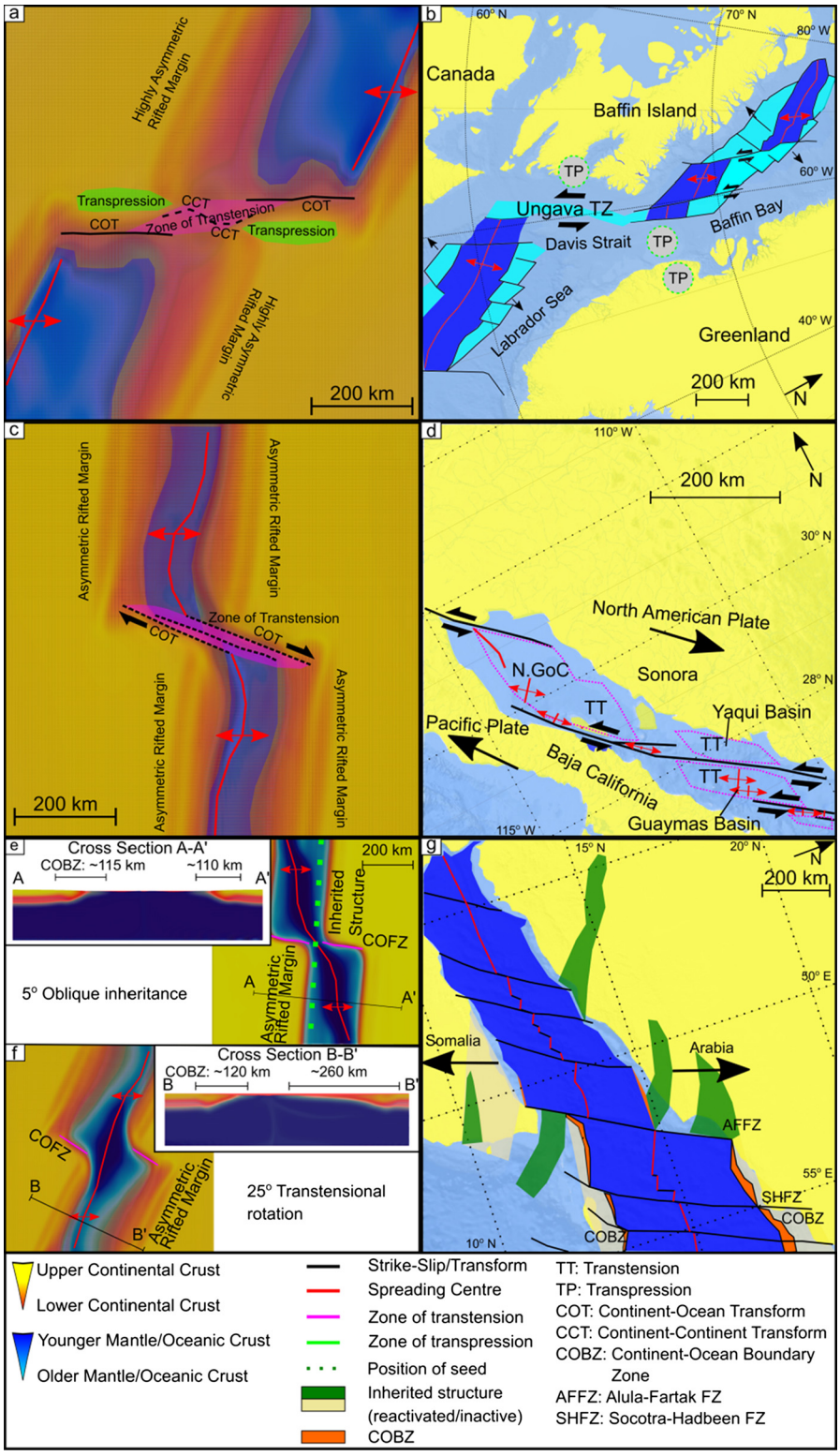

Fig. 8. Comparison with natural examples. a-b) Comparison of a -25^{o} transpressional rotated model snapshot at 20 (+5) Myr with the Davis Strait. Note the zones of compression/transpression within the outer corners of the continent-ocean transforms shown in green; in the natural example, similar areas are indicated with grey circles marked TP (location of transpression from Peace et al., 2017). Also note the transtensional zone shown in pink between the two segments of the COT due to the nature of the rotation. c-d) Comparison of a 5^{o} transtensional rotated model snapshot at 10 (+5) Myr with the Gulf of California. Note the zone of transtension in the model shown in pink; in the natural example, similar areas are marked with dashed pink outlines. e-g) Comparison of a 5^{o} transtensional oblique inheritance model snapshot at 15 Myr and a 25^{o} transtensional rotated model snapshot at 20+5 Myrs with the Gulf of Aden (from Leroy et al., 2012; Bellahsen et al., 2013). Note the similarity in the general oblique rift trend with the rotated model, and the margin asymmetry shown in the inset cross-sections in the rotated model and in orange colour in the natural example (for a zoomed in version of the cross-sections refer to Suppl. Figures S21 and S24).

Suppl. Figure S1), and is consistent with most physical and numerical studies (e.g., a spacing of 4H in Allken et al. (2012) and > 4H in Le Pourhiet et al. (2017)). Such spacing allows the build-up of strain in the tips of the rift structures and the production of transform faults. Zwaan and Schreurs (2017) did not observe transform faults developing in a similar set-up, but used a much smaller spacing of 2H. Yet, in accordance with Zwaan and Schreurs (2017), we also found that an inherited structure located at a high negative (or transpressional) angle (such as the $\theta = -45^{o}$ inherited structure in Fig. 6y) does not produce any rift connectivity, but instead produces two non-interacting distinct rift segments.

4.3. Margin asymmetry

In terms of margin asymmetry, we find that hyper-extension (coupling of upper and lower continental crust) occurs if the plate vector change induces transpression or transtension over the transform and results in stalling rifting, similar to Le Pourhiet et al. (2017). In our oblique inheritance experiments, this asymmetry appears mainly in the higher angle experiments ($>25^{o}$). In Figs. 4p,t, the rift flanks that correspond to the inside corners of the transform are wider than their outside corner counterparts. The inverse happens in Figs. 6o,t, where the outside corner flanks are hyper-extended. Similarly, in our rotated models, hyper-extension occurs on the outside corner rift flank in a positive θ rotation (e.g., Figs. 5 after 15+5 Myr). On the other hand, when a negative θ rotation occurs, these wide zones of diffuse strain occur in the inside corner rift flanks (e.g., Figs. 7 after 20+5 Myr, with cross-sections of the margins shown in Suppl. Figures S20,24,28 & 32). Nonn et al. (2017) provide a potential explanation for this, suggesting rift migration might be responsible for hyper-extension and margin asymmetry. Migration is observed in the positive θ oblique inheritance models, where spreading migrates clockwise, leaving behind a hyperextended margin (comparing 5 Myr and 10 Myr in Fig. 5 and Suppl. Figure S22). Migration also occurs in the other models, but in the region of exposed mantle. Similarly, Le Pourhiet et al. (2017) observe higher continental crust asymmetry across the rift flanks, which they attributed to an already-weakened lower crust in a rift-transform-rift setting. This compares to our rotational models, where the continental crust has already been weakened by the previous orthogonal extension and is then re-mobilised to accommodate asymmetry. When the crust is undisturbed, asymmetry is focused on the oceanic domain (e.g., Le Pourhiet et al., 2017), as is the case in our oblique inheritance models where the crust is not "disturbed" by a previous event of orthogonal extension.

As discussed in Section 4.1.3, another factor that shapes rifted margin asymmetry and evolution is magmatism. If our models included magmatism, we would expect the magmatism in magma-rich margins to be concentrated in zones of hyper-extension thinning (e.g., Mohriak and Leroy, 2013; Koopmann et al., 2016; Peace et al., 2016), altering their rheology and potentially amplifying the hyper-extension. The changes for magma-poor margins are naturally expected to be minimal. However, it is difficult to correlate the width of a rifted margin directly with volcanism (Tugend et al., 2018). A number of previous workers who have investigated margin asymmetry considering magmatic emplacement interpret their results as fundamentally controlled by simple shear rifting, with magmatism controlled by the amount and location of crustal thinning (e.g., Mohriak and Leroy, 2013 on the S. and N. Atlantic, Red Sea and Gulf of Aden; Koopmann et al., 2016 on the S. Atlantic; Peace et al., 2016 on the Labrador Sea). Thinning in a simple shear system is asymmetric; therefore the magmatism is asymmetric. Within this framework, the tectonic structure is the primary driver of asymmetry, so our purely tectonic models should capture the first-order factors affecting margin asymmetry and COBZ width.

4.4. Oblique inheritance versus rotation

We observe that in the case of a negative, transpressional angle change between the oblique inheritance or plate motion vector and the extension direction, the duration of transform margin activity increases substantially (Fig. 9). This is probably due to the juxtaposition of a larger portion of continental crust across the transform imposed by the kinematic boundary conditions, which delays the surface linkage between the two spreading centres. This agrees with Ammann et al. (2018), who found that long transform fault formation is favoured by high obliquity. It is worth noting that, for this set of experiments, the transform margin always remains parallel to sub-parallel to the extension direction (Figs. 6, 7, and 8a).

In positive θ transtensional models, an increasing angle results in shorter duration of transform margin activity. Furthermore, spreading over the rift part of the seeds is delayed with increasing angle of rotation. However, the sigmoidal transtensional zone created above the transform seeds becomes wider in the centre with increasing positive rotation angle (Fig. 4 after 15 Myr and Fig. 5 after 15+5 Myr). This sigmoidal opening style of transtensional oblique inheritance and rotation experiments resembles that observed in Brune and Autin (2013) when they applied oblique extension to an inherited structure in the crust. This can be attributed to the response of the transform segment to the far-field extension. Rifting and subsequent spreading along that intersection is preferred due to the orientation of the pre-existing structures. As θ increases, the spreading component over the rift seeds becomes smaller, while over the transform seed it becomes larger.

Finally, comparing the oblique inheritance and relative plate rotation results, it becomes evident that introducing a rotation to the model delays the ocean-ocean breakthrough across the transform margin, meaning the margin is active for longer (Fig. 9). In our models, this difference is about 5 Myr for positive angles, which is the duration of the orthogonal rifting stage. However, the difference is much greater for negative angles of rotation (Fig. 9). In the transpressional models, stress and strain patterns need to rearrange and cross-cut the pre-existing tectonic fabric, making the transform zones active for longer. In a transtensional regime, this rearrangement would occur faster as the structures need to only re-orient themselves to the new extension direction. A more detailed view of this evolution can be seen in the analogue models of Farangitakis et al. (2019), where a relative plate rotation leads to wide zones of transtension and transpression.

In Fig. 9, we show our model results of transform margin activity and rotation angle alongside a compilation of various transform margin age ranges from Mercier de Lépinay et al. (2016) and obliquity/rotation ranges from Jeanniot and Buiter (2018) (with adjustments for the Gulf of California from Umhoefer et al., 2018 and Farangitakis et al., 2019; for the Tanzania Coastal Basin (TCB) from Farangitakis et al., 2019; and for the De Geer-Spitzbergen transform from Doré et al., 2016). We observe that more transforms fall into a zone defined by the relative plate rotation experiments than by a single phase rift dominated by inheritance. The exceptions are: the Voring Margin, which falls below the oblique inheritance trend line (very high transtensional angle resulting in a short-lived transform; Doré et al., 2016; Jeanniot and Buiter, 2018); and the TCB and De Geer Line, located above the relative rotation trend line. The TCB accommodated motion between supercontinents and is thus much larger scale than the others (Farangitakis et al., 2019), while the polyphase evolution of the De Geer Line is dominated by multiple changes in relative plate motion and far field-forces around the Arctic (according to Doré et al., 2016).

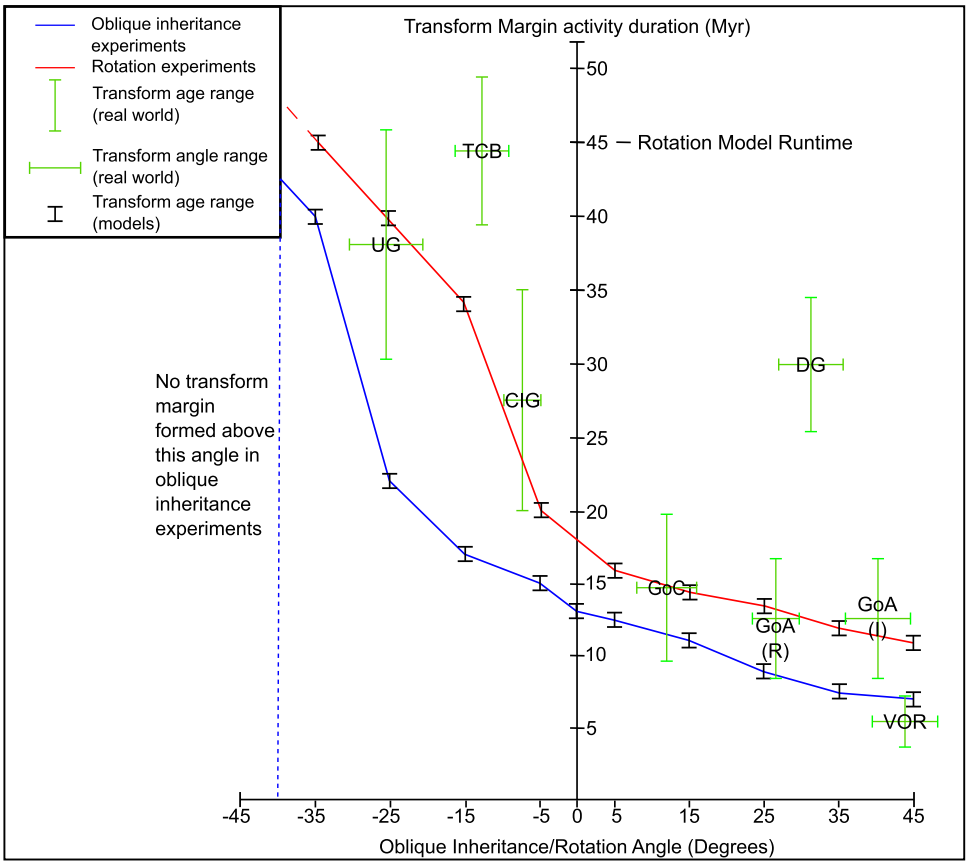

Fig. 9. Comparison between duration of transform margin activity between the oblique inheritance (blue) and rotation (red) experiments versus their angle. Selected transform margins across the world are also shown. Abbreviations: DG: De Geer Transform, TCB: Tanzania Coastal Basin, UG: Ungava Transform Zone, CIG: Cote d'Ivoire-Ghana Transform Marin, GoC: Gulf of California, GoA: Aden Gulf, VOR: Voring Margin.

The natural examples in Fig. 9 provide a qualitative comparison between oblique inheritance and changes in relative plate motion. Our models use a generalised continental lithosphere rheology and do not vary its strength, thickness, mantle temperature or the depth or dip of the inheritance fabric. This generalised model set-up cannot provide as close a match for a specific natural example as area-specific studies (e.g., Brune and Autin, 2013 for the Gulf of Aden). However, despite this, most of the natural examples plot on the rotation trendline, potentially suggesting changes in relative plate motion influenced their evolution (Fig. 9).

A particularly good example of this is given by the Gulf of Aden, which has experienced a combination of inheritance, oblique rifting and vector rotation (Bellahsen et al., 2013). We have plotted therefore two separate components of rifting for this example: the influence of rotation GoA(R) and the influence of inheritance GoA(I). However, we see that the observed duration of transform is consistent with the rotation trendline, not the inheritance one. As discussed above, our rotational model also produces margin asymmetry very similar to that observed in the Gulf. The 26^{o} spreading direction change thus appears crucial in the Gulf of Aden's evolution and margin structure. This complex example strengthens the emerging trend of Fig. 9: that changes in plate motion play a key role in transform margin evolution and should be considered as equally, or potentially more, important than inheritance.

5. Conclusions

We present a series of experiments replicating oblique structural inheritance and rotational changes in relative plate motion in a rift-transform-rift setting. Our results show good agreement with natural examples in the Ungava Transform Zone, the Gulf of California and the Gulf of Aden (Fig. 8).

High-angle relative plate rotations produce both transtension and transpression along a transform system. We show that the evolution of the Davis Strait can be simulated with a transpressional -25° relative plate rotation with respect to the extension direction, resulting in a diffuse zone of transtension where the Ungava Fracture Zone is located and transpression on the inside corners of the COT (Fig. 8a-b).

In a transtensional setting, the obliquity introduced by even a small rotation of existing orthogonal extension results in sigmoidal to rhomboidal opening along the transform margin. This is similar (for the smaller angles) to the evolution of the Gulf of California, where en-echelon pull-aparts developed from south to north and are now evolving into ridge-transform segments (Fig. 8c-d).

Furthermore, we find that relative plate rotations can lead to rifted margin asymmetry. We compare the ocean-continent transition zone width of the Gulf of Aden to both oblique inheritance and rotation models. The width of the ocean-continent transition zone in the rotation models closely matches that of the Gulf of Aden, where the outside corners of the rift-transform intersection are significantly wider than the inside ones (Fig. 8e-f).

We conclude that introducing a relative plate rotation in our models results in a longer transform margin activity lifespan and delayed spreading along the entire margin (Fig. 9). This is due to the delay caused by the reorganisation of the diffuse strain patterns associated with transtension and transpression when a rotational change in plate motion occurs.

Therefore, the effects of relative plate rotations on rift-transform intersections should be considered alongside inheritance when understanding the evolution of a margin.

Declaration of competing interest

The authors declare that they have no known competing financial interests or personal relationships that could have appeared to influence the work reported in this paper.

Acknowledgements

The work contained in this paper contains work conducted during a PhD study undertaken as part of the Natural Environment Research Council (NERC) Centre for Doctoral Training (CDT) in Oil & Gas [grant number NEM00578X/1]. It is co-sponsored by Durham University whose support is gratefully acknowledged. PJH is funded by the EU Horizon 2020 research and innovation programme under the MSCA grant agreement 749664. LMK is supported by a Royal Society of Edinburgh Personal Research Fellowship funded by The Scottish Government. This work made use of the facilities of the Hamilton HPC Service of Durham University and the ARCHER UK National Supercomputing Service (http://www.archer.ac.uk). We thank the Computational Infrastructure for Geodynamics (geodynamics.org), which is funded by the National Science Foundation under Awards EAR-0949446 and EAR-1550901, for supporting the development of ASPECT. Data and input files are available at https://github.com/pfarangitakis/ASPECT-PRM.

Appendix A. Supplementary material

Supplementary material related to this article can be found online at https://doi.org/10.1016/j.epsl.2020.116277.

References

Allken, V., Huismans, R.S., Thieulot, C., 2012. Factors controlling the mode of rift interaction in brittle-ductile coupled systems: a 3D numerical study. Geochem. Geophys. Geosyst. 13 (5). https://doi.org/10.1029/2012GC004077.

Ammann, N., Liao, J., Gerya, T., Ball, P., 2018. Oblique continental rifting and long transform fault formation based on 3D thermomechanical numerical modeling. Tectonophysics 746, 106–120. https://doi.org/10.1016/j.tecto.2017.08.015.

Autin, J., Bellahsen, N., Leroy, S., Husson, L., Beslier, M., d'Acremont, E., 2013. The role of structural inheritance in oblique rifting: insights from analogue models and application to the Gulf of Aden. Tectonophysics 607, 51–64. https://doi.org/10.1016/j.tecto.2013.05.041.

Basile, C., 2015. Transform continental margins — part 1: Concepts and models. Tectonophysics 661, 1–10. https://doi.org/10.1016/j.tecto.2015.08.034.

Bellahsen, N., Leroy, S., Autin, J., Razin, P., d'Acremont, E., Sloan, H., Pik, R., Ahmed, A., Khanbari, K., 2013. Pre-existing oblique transfer zones and transfer/transform relationships in continental margins: new insights from the southeastern Gulf of Aden, Socotra island, Yemen. Tectonophysics 607, 32–50. https://doi.org/10.1016/j.tecto.2013.07.036.

Bennett, S.E.K., Oskin, M.E., 2014. Oblique rifting ruptures continents: example from the Gulf of California shear zone. Geology 42 (3), 215–218. https://doi.org/10.1130/G34904.1.

Bos, B., Spiers, C.J., 2002. Frictional-viscous flow of phyllosilicate-bearing fault rock: microphysical model and implications for crustal strength profiles. J. Geophys. Res., Solid Earth 107. https://doi.org/10.1029/2001JB000301. ECV 1-1; ECV 1-13.

Bosworth, W., 1986. Comment and reply on "Detachment faulting and the evolution of passive continental margins" COMMENT. Geology 14 (10), 890–891.

Brune, S., Autin, J., 2013. The rift to break-up evolution of the Gulf of Aden: insights from 3D numerical lithospheric-scale modelling. Tectonophysics 607, 65–79. https://doi.org/10.1016/j.tecto.2013.06.029.

Brune, S., Popov, A.A., Sobolev, S.V., 2012. Modeling suggests that oblique extension facilitates rifting and continental break-up. J. Geophys. Res., Solid Earth 117. https://doi.org/10.1029/2011JB008860.

Brune, S., Williams, S.E., Müller, R.D., 2018. Oblique rifting: the rule, not the exception. Solid Earth 9, 1187–1206. https://doi.org/10.5194/se-9-1187-2018.

Chapman, D.S., 1986. Thermal gradients in the continental crust. Geol. Soc. (Lond.) Spec. Publ. 24 (1), 63–70. https://doi.org/10.1144/GSL.SP.1986.024.01.07.

Doré, A.G., Lundin, E.R., Gibbons, A., Sømme, T.O., Tørudbakken, B.O., 2016. Transform margins of the Arctic: a synthesis and re-evaluation. Geol. Soc. (Lond.) Spec. Publ. 431 (1), 63–94. https://doi.org/10.1144/SP431.8.

Farangitakis, G.-P., Sokoutis, D., McCaffrey, K.J.W., Willingshofer, E., Kalnins, L.M., Phethean, J.J.J., van Hunen, J., van Steen, V., 2019. Analogue modeling of plate rotation effects in transform margins and rift-transform intersections. Tectonics 38 (3), 823–841. https://doi.org/10.1029/2018TC005261.

Gerya, T.V., 2013. Three-dimensional thermomechanical modeling of oceanic spreading initiation and evolution. Phys. Earth Planet. Inter. 214, 35–52. https://doi.org/10.1016/j.pepi.2012.10.007.

Glerum, A., Thieulot, C., Fraters, M., Blom, C., Spakman, W., 2018. Nonlinear viscoplasticity in ASPECT: benchmarking and applications to subduction. Solid Earth 9 (2), 267–294. https://doi.org/10.5194/se-9-267-2018.

Heister, T., Dannberg, J., Gassmöller, R., Bangerth, W., 2017. High accuracy mantle convection simulation through modern numerical methods – II: realistic models and problems. Geophys. J. Int. 210 (2), 833–851. https://doi.org/10.1093/gji/ggx195.

Heron, P.J., Peace, A.L., McCaffrey, K.J., Welford, J.K., Wilson, R., van Hunen, J., Pysklywec, R.N., 2019. Segmentation of rifts through structural inheritance: creation of the Davis strait. Tectonics 38, 1–20. https://doi.org/10.1029/2019TC005578.

Hirth, G., Kohlstedt, D., 2004. In: Eiler, J. (Ed.), Rheology of the Upper Mantle and the Mantle Wedge: a View from the Experimentalists. Wiley. Retrieved from https://doi.org/10.1029/138GM06.

Huismans, R., Beaumont, C., 2011. Depth-dependent extension, two-stage breakup and cratonic underplating at rifted margins. Nature 473, 74–78. https://doi.org/10.1038/nature09988.

Illsley-Kemp, F., Bull, J.M., Keir, D., Gerya, T., Pagli, C., Gernon, T., Ayele, A., Goitom, B., Hammond, J.O.S., Kendall, J.M., 2018. Initiation of a proto-transform fault prior to seafloor spreading. Geochem. Geophys. Geosyst. 19 (12), 4744–4756. https://doi.org/10.1029/2018GC007947.

Jeanniot, L., Buiter, S.J.H., 2018. A quantitative analysis of transtensional margin width. Earth Planet. Sci. Lett. 491, 95–108. https://doi.org/10.1016/j.epsl.2018.03.003.

Kachanov, L.M., 2004. Fundamentals of the Theory of Plasticity. Dover Publications, Inc.

Karato, S., 2008. Deformation of Earth Materials: An Introduction to the Rheology of Solid Earth. Cambridge University Press, Cambridge.

Koopmann, H., Schreckenberger, B., Franke, D., Becker, K., Schnabel, M., 2016. The late rifting phase and continental break-up of the southern south Atlantic: the mode and timing of volcanic rifting and formation of earliest oceanic crust. Geol. Soc. (Lond.) Spec. Publ. 420 (1), 315–340. https://doi.org/10.1144/SP420.2.

Kronbichler, M., Heister, T., Bangerth, W., 2012. High accuracy mantle convection simulation through modern numerical methods. Geophys. J. Int. 191 (1), 12–29. https://doi.org/10.1111/j.1365-246X.2012.05609.x.

Le Pichon, X., Hayes, D.E., 1971. Marginal offsets, fracture zones, and the early opening of the south atlantic. J. Geophys. Res. 76 (26), 6283–6293. https://doi.org/10.1029/JB076i026p06283.

Le Pourhiet, L., May, D.A., Huille, L., Watremez, L., Leroy, S., 2017. A genetic link between transform and hyper-extended margins. Earth Planet. Sci. Lett. 465, 184–192. https://doi.org/10.1016/j.epsl.2017.02.043.

Leroy, S., Razin, P., Autin, J., Bache, F., d, Acremont E., Watremez, L., et al., 2012. From rifting to oceanic spreading in the gulf of aden: a synthesis. Arab. J. Geosci. 5 (5), 859–901. https://doi.org/10.1007/s12517-011-0475-4.

Lorenzo, J.M., 1997. Sheared continent ocean margins: an overview. Geo Mar. Lett. 17 (1), 1–3. https://doi.org/10.1007/PL00007201.

Mercier de Lépinay, M., Loncke, L., Basile, C., Roest, W.R., Patriat, M., Maillard, A., De Clarens, P., 2016. Transform continental margins – part 2: a worldwide review. Tectonophysics 693 (Part A), 96–115. https://doi.org/10.1016/j.tecto.2016.05.038.

Mohriak, W.U., Leroy, S., 2013. Architecture of rifted continental margins and breakup evolution: Insights from the south Atlantic, north Atlantic and Red Sea–Gulf of Aden conjugate margins. Geol. Soc. (Lond.) Spec. Publ. 369 (1), 497–535. https://doi.org/10.1144/SP369.17.

Morrow, T.A., Mittelstaedt, E., Kim, S., 2019. Are segmented fracture zones weak? Analytical and numerical models constrain anomalous bathymetry at the Clarion and Murray fracture zones. Earth Planet. Sci. Lett. 512, 214–226. https://doi.org/10.1016/j.epsl.2019.02.010.

Naliboff, J., Buiter, S.J.H., 2015. Rift reactivation and migration during multiphase extension. Earth Planet. Sci. Lett. 421, 58–67. https://doi.org/10.1016/j.epsl.2015.03.050.

Nonn, C., Leroy, S., Khanbari, K., Ahmed, A., 2017. Tectono-sedimentary evolution of the eastern Gulf of Aden conjugate passive margins: narrowness and asymmetry in oblique rifting context. Tectonophysics 721, 322–348. https://doi.org/10.1016/j.tecto.2017.09.024.

Oakey, G.N., Chalmers, J.A., 2012. A new model for the Paleogene motion of Greenland relative to North America: plate reconstructions of the Davis Strait and Nares Strait regions between Canada and Greenland. J. Geophys. Res., Solid Earth 117. https://doi.org/10.1029/2011JB008942.

Peace, A., McCaffrey, K., Imber, J., Phethean, J., Nowell, G., Gerdes, K., Dempsey, E., 2016. An evaluation of Mesozoic rift-related magmatism on the margins of the Labrador Sea: implications for rifting and passive margin asymmetry. Geosphere 12 (6), 1701–1724. https://doi.org/10.1130/GES01341.1.

Peace, A., McCaffrey, K.J.W., Imber, J., van Hunen, J., Hobbs, R.W., Wilson, R., 2017. The role of pre-existing structures during rifting, continental breakup and transform system development, offshore west Greenland. Basin Res. 30 (3). https://doi.org/10.1111/bre.12257.

Persaud, P., Stock, J.M., Steckler, M.S., Martín-Barajas, A., Diebold, J.B., González-Fernández, A., Mountain, G.S., 2003. Active deformation and shallow structure of the Wagner, Consag, and Delfín basins, Northern Gulf of California, Mexico. J. Geophys. Res., Solid Earth 108 (B7), 2355. https://doi.org/10.1029/2002JB001937.

Reid, D.I., Jackson, H.R., 1997. A review of three transform margins off eastern Canada. Geo Mar. Lett. 17 (1), 87–93. https://doi.org/10.1007/s003670050012.

Rose, I., Buffett, B., Heister, T., 2017. Stability and accuracy of free surface time integration in viscous flows. Phys. Earth Planet. Inter. 262, 90–100. https://doi.org/10.1016/j.pepi.2016.11.007.

Rutter, E.H., Brodie, K.H., 2004. Experimental intracrystalline plastic flow in hot-pressed synthetic quartzite prepared from brazilian quartz crystals. J. Struct. Geol. 26 (2), 259–270. https://doi.org/10.1016/S0191-8141(03)00096-8.

Rybacki, E., Gottschalk, M., Wirth, R., Dresen, G., 2006. Influence of water fugacity and activation volume on the flow properties of fine-grained anorthite aggregates. J. Geophys. Res., Solid Earth 111. https://doi.org/10.1029/2005JB003663.

Thieulot, C., 2011. FANTOM: two- and three-dimensional numerical modelling of creeping flows for the solution of geological problems. Phys. Earth Planet. Inter. 188 (1), 47–68. https://doi.org/10.1016/j.pepi.2011.06.011.

Tugend, J., Gillard, M., Manatschal, G., Nirrengarten, M., Harkin, C., Epin, M.E., Sauter, D., Autin, J., Kusznir, N., McDermott, K., 2018. Reappraisal of the magma-rich versus magma-poor rifted margin archetypes. Geol. Soc. (Lond.) Spec. Publ. 476, SP476.9. https://doi.org/10.1144/SP476.9.

Umhoefer, P.J., Darin, M.H., Bennett, S.E.K., Skinner, L.A., Dorsey, R.J., Oskin, M.E., 2018. Breaching of strike-slip faults and successive flooding of pull-apart basins to form the Gulf of California seaway from ca. 8–6 ma. Geology 46 (8), 695–698. https://doi.org/10.1130/G40242.1.

Willett, S.D., 1992. Dynamic and kinematic growth and change of a coulomb wedge. In: McClay, K.R. (Ed.), Thrust Tectonics. Springer Netherlands, Dordrecht, pp. 19–31. Retrieved from https://doi.org/10.1007/978-94-011-3066-0_2.

Wilson, J.T., 1965. A new class of faults and their bearing on continental drift. Nature 207 (4995), 343–347. https://doi.org/10.1038/207343a0.

Wilson, R.W., Klint, K.E.S., van Gool, J.A.M., McCaffrey, K.J.W., Holdsworth, R.E., Chalmers, J.A., 2006. Faults and fractures in central west Greenland: onshore expression of continental break-up and sea-floor spreading in the Labrador - Baffin bay sea. Geol. Surv. Denmark and Greenland Bull. 11, 185–204.

Zwaan, F., Schreurs, G., 2017. How oblique extension and structural inheritance influence rift segment interaction: insights from 4D analog models. Interpret. 5 (1), 119–138. https://doi.org/10.1190/INT-2016-0063.1.